

# Simple and effective descriptor for measuring the nonlinear optical responses of atomic clusters

*Quanjie Zhong\**

School of Materials Science and Physics, China University of Mining and Technology,  
Xuzhou 221116, Jiangsu Province, China

E-mail address: [quanjiezhong@cumt.edu.cn](mailto:quanjiezhong@cumt.edu.cn)

## ABSTRACT

Atomic clusters, a form of matter that is intermediate between atomic and condensed states, feature tremendous geometrical and chemical-compositional flexibilities. Unlike inorganic crystals and organic molecules, atomic clusters escape the well-established physical model developed decades ago for predicting nonlinear optical properties, which presents opportunities for achieving currently unattainable nonlinear optical performances. However, clear conceptual guidelines for designing specific geometries with maximal nonlinear optical responses are lacking. Herein, a simple and efficient length descriptor for determining the optical responses of atomic-cluster isomers is reported. The response charge, a newly introduced concept, reveals that the length tunes the optical performance by controlling electron delocalization in atomic-cluster isomers, with the one-dimensional geometry providing optimal optical performance. Finally, the optical behaviors of one-dimensional geometries are quantitatively rationalized by the response charge, providing a clear physical picture. The intuitive rule developed herein is expected to powerfully accelerate the rational design of novel nonlinear optical materials.

## INTRODUCTION

Atomic clusters contain several to hundreds of atoms and bridge the gap between atoms and condensed matter in terms of physical and chemical characteristics<sup>1</sup>. With their continuously tunable geometric size and chemical composition, and absence of periodic

constrains<sup>2,3</sup>, atomic clusters offer tremendous opportunities for designing high-performance nonlinear optical materials<sup>4-7</sup>. Numerous studies aimed at screening atomic clusters with outstanding nonlinear optical properties and predicting favorable geometries for nonlinear optical responses have been reported<sup>8-11</sup>. For a specified atomic cluster, state-of-the-art density functional theory and the wavefunction method can accurately evaluate its nonlinear optical performance<sup>12,13</sup>. However, accurately identifying the optimal geometry is challenging because atomic clusters exist in countless isomeric forms. A simple physical model that provides general rules for predicting the nonlinear optical response behaviors of atomic clusters is essential to efficiently explore the vast geometric space, rather than relying solely on density functional theory or wavefunction theory simulations.

In general, the nonlinear optical coefficients of bulk materials are qualitatively determined from their bandgaps owing to their inverse relationships, and nonlinear optical crystals with large susceptibility coefficients have been prepared according to this principle<sup>14,15</sup>. For organic molecules, the multi-level model derived from the sum-over-state formula similarly reveals that narrow HOMO–LUMO gaps lead to strong nonlinear optical effects<sup>16,17</sup>, which has stimulated the design and synthesis of various organic molecules with D– $\pi$ –A structures<sup>18-20</sup>. Although the bandgap or HOMO–LUMO gap descriptors have been used with great success for decades to understand nonlinear optical behaviors, atomic clusters do not follow the general trends observed for traditional nonlinear optical materials<sup>21</sup>. Statistically, the HOMO–LUMO gap of an atomic clusters is very weakly correlated to its polarizability ( $\alpha$ ) and second-order hyperpolarizability ( $\gamma$ ) (Figure S3). Specifically, slight positive correlations are often observed between  $\alpha$ ,  $\gamma$ , and the HOMO–LUMO gap, contrary to the predictions of the multi-level model. Atomic clusters usually lack well-defined characteristic excited states (i.e., excited states with low excitation energies, and large oscillator strengths and dipole moments), consequently, the multi-level model struggles to adequately explain the nonlinear optical responses of atomic

clusters. To address the dilemmas encountered by the traditional model, bonding analyses were introduced to understand the nonlinear optical behaviors observed for atomic clusters<sup>22,23</sup>. While bonding patterns provide meaningful insight into the nonlinear optical responses of ultra-small atomic clusters<sup>24</sup>, bonding analyses are challenging for medium-sized atomic cluster owing to their complex bonding patterns. In particular, local bonding information fails to reveal the overall nonlinear optical response characteristics. Consequently, the bonding characteristics provide insufficient general physical insight into the factors that govern the nonlinear optical behaviors of an atomic cluster.

Previous research revealed that elongated geometries generally exhibit enhanced nonlinear optical responses compared to compact ones, which is an interesting discovery. Herein, the one-dimensional geometry is demonstrated to be the optimal linear and nonlinear optical response solution for an atomic cluster using silicon, phosphorus, and sulfur isomers as model systems. Response-charge analysis reveals that lengthening the atomic-cluster isomer enhances electron delocalization and promotes positive and negative response-charge separation, thereby improving the linear and nonlinear optical performance of the atomic-cluster isomer. Importantly, this study establishes a clear guideline for theoreticians and experimentalists when constructing high-performance nonlinear optical materials without the need for expensive and complex simulations.

## RESULTS AND DISCUSSIONS

Single-element silicon, phosphorus, and sulfur isomers containing 20 atoms were selected as model systems and the linear and nonlinear optical behaviors of their atomic clusters were investigated. Static orientationally average polarizability ( $\alpha_{ave}$ ) and second-order hyperpolarizability ( $\gamma_{ave}$ ) were investigated to reveal the intrinsic linear and nonlinear optical responses of atomic clusters while avoiding dispersion effects. A series of measurements were used to establish a reliable data set for analyzing the linear and nonlinear optical responses of atomic clusters (Tables S1–S3, Figures S1 and S2). As shown in Figure 1,  $\alpha_{ave}$  and  $\gamma_{ave}$  are significantly positively correlated with the  $x$ -length, as

defined by the moment of inertia of atomic-cluster isomers, with the statistical data exhibiting three main characteristics: (1)  $\alpha_{ave}$  and  $\gamma_{ave}$  are linearly and exponentially dependent on the  $x$ -length, respectively, in the examined range; (2) the  $\alpha_{ave}$  and  $\gamma_{ave}$  values gradually decline when moving from silicon to phosphorus and sulfur at the same  $x$ -length; and (3) as a whole,  $\alpha_{ave}$ ,  $\gamma_{ave}$ , and  $x$ -length gradually become less correlated when moving from silicon to phosphorus and sulfur.

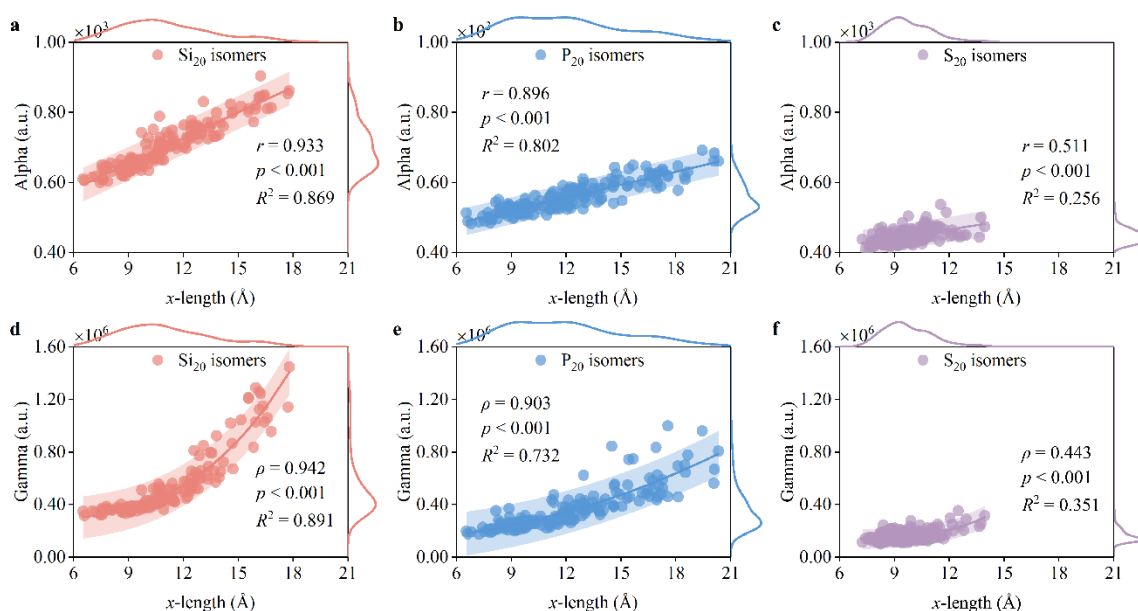


**Figure 1. Measuring the linear and nonlinear optical responses of atomic-cluster isomers using the  $x$ -length descriptor.** a–c, Linear correlations between  $\alpha_{ave}$  and  $x$ -length and d–f exponential correlations between  $\gamma_{ave}$  and  $x$ -length for (a, d) silicon ( $n = 151$ ), (b, e) phosphorus ( $n = 169$ ), and (c, f) sulfur ( $n = 150$ ) isomers. Linear and exponential correlations were assessed using Pearson ( $r$ ) and Spearman ( $\rho$ ) correlation coefficients, respectively;  $p$  and  $R^2$  represent statistical significance and the coefficient of determination of the fitted data, respectively. Colored regions correspond to prediction bands, each with a confidence level of 95%.

Previous studies have revealed that a linear correlation exists between  $\alpha_{ave}$  and the molecular volume<sup>25,26</sup>, while  $\gamma_{ave}$  increase exponentially with increasing chain length for  $\pi$ -conjugated molecules<sup>27,28</sup>. In this work, the significant positive correlations between  $\alpha_{ave}$ ,

$\gamma_{\text{ave}}$  and  $x$ -length are actually surprising because all clusters contain 20 atoms, which reveals that the geometry modulates the linear and nonlinear optical responses. Silicon clusters were selected as analysis examples. Formally,  $\alpha_{\text{ave}}$  is determined from the  $\alpha_{xx}$ ,  $\alpha_{yy}$ , and  $\alpha_{zz}$  components. As shown in Figure 2a,  $\alpha_{xx}$  is linearly dependent on  $x$ -length. Statistically, increasing  $x$ -length forces the  $y$ - and  $z$ -length to decline because the number of atoms is constant; however, relatively limited decrements in  $y$ - and  $z$ -length were observed. In addition, the  $\alpha_{yy}/\alpha_{zz}$  value varies more gently with  $y/z$ -length than the  $\alpha_{xx}$  value does in response to  $x$ -length. Consequently, the higher  $\alpha_{xx}$  value more than offsets the lower  $\alpha_{yy}$  and  $\alpha_{zz}$  values. For instance, the  $\alpha_{xx}$  value increases significantly from 600 to 1600 a.u. with  $x$ -length, while the  $\alpha_{yy}$  and  $\alpha_{zz}$  values decrease slightly from 700 to 500 a.u., and 600 to 400 a.u., respectively. Actually,  $\alpha_{yy}$  and  $\alpha_{zz}$  are approximated as constants:  $\alpha_{xx}$  causes  $\alpha_{\text{ave}}$  to evolve linearly with  $x$ -length. In a similar manner to  $\alpha_{\text{ave}}$ ,  $\gamma_{\text{ave}}$  is determined by the  $\gamma_{xxxx}$ ,  $\gamma_{yyyy}$ ,  $\gamma_{zzzz}$ ,  $\gamma_{xxyy}$ ,  $\gamma_{xxzz}$ , and  $\gamma_{yyzz}$  components. As shown in Figure 2d,  $\gamma_{xxxx}$  depends exponentially on  $x$ -length. Clearly,  $\gamma_{xxxx}$  increases considerably, whereas the other components decrease to an extremely limited extent, thereby leading to  $\gamma_{\text{ave}}$  evolving exponentially with  $x$ -length.

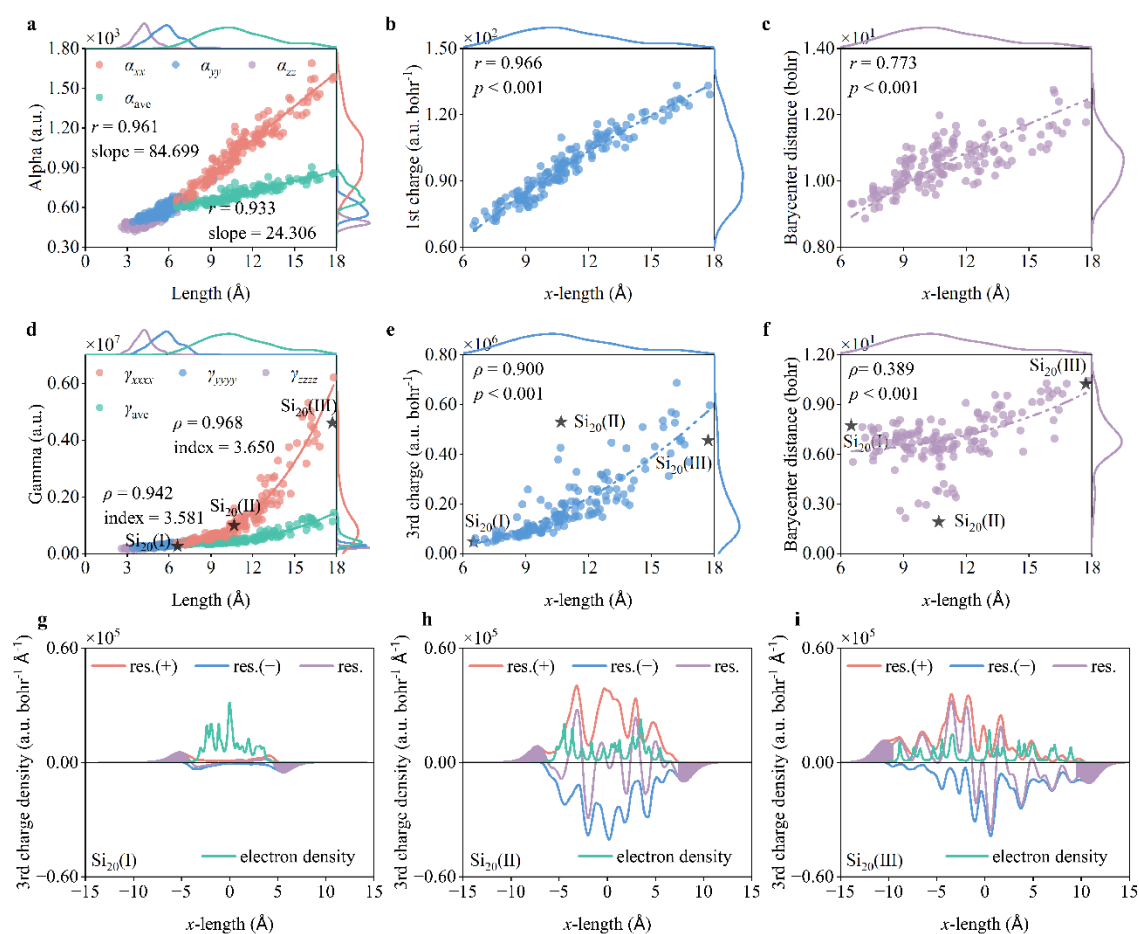


**Figure 2. Mechanism for regulating the linear and nonlinear optical responses of silicon isomers, based on the  $x$ -length descriptor.** **a**, Statistical dependences of  $\alpha_{xx}$ ,  $\alpha_{yy}$ ,  $\alpha_{zz}$ , and  $\alpha_{ave}$  on length. **b**, Statistical dependence of  $Q_x^{(1)}$  on  $x$ -length. **c**, Statistical dependence of  $\Delta r_x^{(1)}$  on  $x$ -length. **d**, Statistical dependences of  $\gamma_{xxxx}$ ,  $\gamma_{yyyy}$ ,  $\gamma_{zzzz}$ , and  $\gamma_{ave}$  on length. **e**, Statistical dependence of  $Q_{xxx}^{(3)}$  on  $x$ -length. **f**, Statistical dependence of  $\Delta r_x^{(3)}$  on  $x$ -length. Note that the dashed lines in panels b, c, e, and f are trend lines rather than fitted curves. **g**, **h**, **i**, 3rd-order response-charge and electron-density curves for the (**g**) Si<sub>20</sub>(I), (**h**) Si<sub>20</sub>(II), and (**i**) Si<sub>20</sub>(III) clusters along the  $x$ -direction. Res.(+) and Res.(−) represent the positive and negative 3rd-order response-charge-density curves, respectively.  $Q_{xxx}^{(3)}(+)$  and  $|Q_{xxx}^{(3)}(-)|$  are precisely equal for electrically neutral systems; hence, the areas enclosed by the positive and negative 3rd-order response-charge-density curves and the  $x$ -axis always

match for any atomic cluster. Here,  $Q_{xxx}^{(3)}$ ,  $Q_{xxx}^{(3)(+)}$ , and  $Q_{xxx}^{(3)(-)}$  satisfy the following quantitative relationship:  $Q_{xxx}^{(3)} = Q_{xxx}^{(3)(+)} = |Q_{xxx}^{(3)(-)}|$ . Res. refers to the difference between the positive and negative 3rd-order response-charge-density curves. Purple regions show the spatial distribution of  $Q_{ext,xxx}^{(3)}$  along the  $x$ -axis, and its area reflects the value of  $Q_{ext,xxx}^{(3)}$ . Notably, the  $y$ -axes that correspond to electron-density curves in panels g, h, and i are not displayed for aesthetic reasons; they have the same coordinate scale.

To explain why  $\alpha_{xx}$  and  $\gamma_{xxxx}$  depend linearly and exponentially on the  $x$ -length, respectively, response charges  $Q^{(n)}$  ( $dQ^{(n)} = \rho^{(n)}dV$ ) are introduced as a new concept. Here,  $n$  is a non-negative integer,  $Q^{(0)}$  corresponds to the electron charge,  $Q^{(1)}$  and  $Q^{(3)}$  refer to the 1st- and 3rd-order response charges, respectively,  $\rho^{(n)}$  is the  $n$ th-order response density of electrons (also known as “hyperpolarizability density” in the general literature<sup>29</sup>); this value is obtained by differentiating the electron density with respect to the external electric field. For electrically neutral systems, the polarizability and second-order hyperpolarizability components ( $\alpha_{ij}$  and  $\gamma_{ijkl}$ ) are accurately described using Equations (1) and (2):

$$\alpha_{il} = Q_i^{(1)}\Delta r_l^{(l)} \quad (1)$$

$$\gamma_{ijkl} = Q_{ijk}^{(3)}\Delta r_l^{(3)} \quad (2)$$

Here,  $Q_i^{(1)}$  is the 1st-order response charge that corresponds to  $\alpha_{ij}$ ,  $Q_{ijk}^{(3)}$  is the 3rd-order response charge that corresponds to  $\gamma_{ijkl}$ ,  $\Delta r_l^{(n)}$  refers to the distance between the positive and negative response-charge distribution centers along the  $l$  direction, and  $i, j, k$  and  $l$  represent one of the Cartesian coordinates  $\{x, y, z\}$ . Clearly,  $\alpha_{xx}$  depends on  $Q_x^{(1)}$  and  $\Delta r_x^{(1)}$ , while  $\gamma_{xxxx}$  is determined by  $Q_{xxx}^{(3)}$  and  $\Delta r_x^{(3)}$ .

Response charges  $Q_x^{(1)}$  and  $Q_{ijk}^{(3)}$  were obtained by numerically differentiating the electron density. Statistically, both  $Q_x^{(1)}$  and  $\Delta r_x^{(1)}$  increase exponentially with the  $x$ -length, with an index value less than unity, which forces  $\alpha_{xx}$  to evolve linearly with the  $x$ -length (Figures 2b and 2c). However,  $Q_{xxx}^{(3)}$  is more weakly correlated with  $x$ -length than  $\gamma_{xxxx}$  (Figure 2e). In particular, pretty-weak correlation exists between  $\Delta r_x^{(3)}$  and  $x$ -length (Figure

2f). Considering the interrelationship between  $\gamma_{xxx}$ ,  $Q_{xxx}^{(3)}$ , and  $\Delta r_x^{(3)}$  ( $\gamma_{xxx} = Q_{xxx}^{(3)} \Delta r_x^{(3)}$ ), these observations are actually surprising. Equation (2) can be rewritten as the sum of two terms; i.e.,  $\gamma_{xxx} = Q_{int,xxx}^{(3)} \Delta r_{int,x}^{(3)} + Q_{ext,xxx}^{(3)} \Delta r_{ext,x}^{(3)}$ , with the former and latter terms representing the contributions of the internal and external 3rd-order response charge to  $\gamma_{xxx}$ , respectively. Here, the internal and external response charges are divided according to the spatial region where the response charge is located. Si<sub>20</sub>(I), Si<sub>20</sub>(II), and Si<sub>20</sub>(III) clusters with obvious particularities were specifically analyzed (Figures 2d to 2f). Among them, the Si<sub>20</sub>(I) cluster possesses the minimum  $x$ -length in all investigated clusters, the Si<sub>20</sub>(II) cluster represents a typical case in which the  $Q_{xxx}^{(3)}$  and  $\Delta r_x^{(3)}$  values deviate from the correlations, the Si<sub>20</sub>(III) cluster possesses a significantly larger  $\gamma_{xxx}$  value than that of the Si<sub>20</sub>(II) cluster while its  $Q_{xxx}^{(3)}$  value is smaller. The response-charge density curves clearly reveal that  $\gamma_{xxx}$  is dominated by the external response charge, while the contribution from the internal response charge is very small owing to its considerably weakly separated positive and negative response-charge centers (Figures 2g to 2i). For the Si<sub>20</sub>(II) cluster,  $Q_{ext,xxx}^{(3)}$  contribute 93.08% to the  $\gamma_{xxx}$  value with only 5.99% of the  $Q_{ext,xxx}^{(3)}/Q_{xxx}^{(3)}$  ratio, leading to a  $\gamma_{xxx}$  value that falls in the middle of the range observed for all investigated clusters, despite possessing a large  $Q_{xxx}^{(3)}$ . Consequently,  $Q_{ext,xxx}^{(3)}$  better reveals how modulating  $x$ -length affects the  $\gamma_{xxx}$  value than  $Q_{xxx}^{(3)}$ , and the  $Q_{ext,xxx}^{(3)}$  and  $\gamma_{xxx}$  ordering are exactly the same for examined three clusters. Static-charge decreases with increasing  $x$ -length near the purple areas, as indicated by the electron-density curves; however,  $Q_{ext,xxx}^{(3)}$  increases with  $x$ -length, which clearly reveal that electron delocalization is enhanced when moving from the Si<sub>20</sub>(I) to Si<sub>20</sub>(II) and Si<sub>20</sub>(III) clusters. Up to this point, a general physical understanding of the significant positive correlations between  $\alpha_{ave}$ ,  $\gamma_{ave}$ , and  $x$ -length was presented.  $X$ -length modulates  $\alpha_{xx}$  and  $\gamma_{xxx}$  by controlling electron delocalization; increasing  $x$ -length raises the response charge, while promoting the separation between the positive and negative response charges leads to elongated geometries that exhibit stronger optical responses than their compact geometries.

Valence electrons that are weakly bound to nuclei induce sensitive nonlinear optical responses in atomic clusters<sup>30</sup>. The nuclear binding strengths experienced by the binding and lone-pair electrons progressively increase when moving from silicon to phosphorus and sulfur, owing to their decreasing atomic radii, and this causes  $\alpha_{ave}$  and  $\gamma_{ave}$  to gradually decline. Meanwhile, the response charge reveals that electron delocalization is attenuated in moving from silicon to phosphorus and sulfur (Figures S5 and S6). Consequently, silicon clusters exhibit enhanced linear and nonlinear optical responses compared to those of phosphorus and sulfur clusters. Notably, the correlations between  $\alpha_{ave}$ ,  $\gamma_{ave}$ , and  $x$ -length are controlled by both physical and non-physical mechanisms. Among them, the physical mechanism, which involves geometries and bonding patterns, causes  $\alpha_{ave}$  and  $\gamma_{ave}$  to intrinsically fluctuate at the same  $x$ -length. In contrast, the non-physical mechanism, which refers to theoretical-method incompleteness, causes the calculated value to deviate from the actual value<sup>31</sup>. The simulated values deviate significantly from the actual values for systems with multi-reference characteristics and are typically overestimated. Because electron delocalization in the cluster is increasingly attenuated in moving from silicon to phosphorus and sulfur, the trend in which  $\alpha_{ave}$  and  $\gamma_{ave}$  increase with increasing  $x$ -length gradually declines, which strengthens the non-physical effect; consequently,  $\alpha_{ave}$ ,  $\gamma_{ave}$ , and  $x$ -length become less correlated.

Since  $\alpha_{ave}$ ,  $\gamma_{ave}$ , and  $x$ -length are significantly correlated, one-dimensional (1D) geometries actually present optimal solutions for both the linear and nonlinear optical responses of atomic clusters. Silicon atoms cannot easily form thermodynamically stable single-element 1D geometries<sup>32</sup>. Here, a new method involving three fragments (T1, T2, and M1) is proposed for assembling 1D silicon geometries that always correspond to minima on the adiabatic potential energy surface (Figure 3a). In contrast, 1D sulfur geometries were experimentally well characterized decades ago<sup>33</sup>. Here, the linear and nonlinear optical responses of 1D silicon with  $D_{2d}$  symmetry and sulfur with a helical geometry were investigated (Figures 3b and 3c). The dependences of  $\alpha_{xx}$  and  $\gamma_{xxxx}$  on  $x$ -

length transition from exponential to linear as  $x$ -length is increased to 100 Å, which implies that the 1D geometries exhibit budding linear and nonlinear optical performance saturation (Figures 3d and 3e). To date, these saturation behaviors have simply been referred to as “delocalized-electron saturation”<sup>34</sup> without a clear physical picture provided, thereby failing to quantitatively explain the linear dependence. Here, the dilemma is addressed using the newly introduced response-charge concept. As discussed earlier, both  $Q_{ext,x}^{(1)}$  and  $Q_{int,x}^{(1)}$  contribute the  $\alpha_{xx}$ , i.e.,  $\alpha_{xx} = Q_{int,x}^{(1)} \Delta r_{int,x}^{(1)} + Q_{ext,x}^{(1)} \Delta r_{ext,x}^{(1)}$ . At the initial  $x$ -length-increasing phase,  $Q_{ext,x}^{(1)}$  primarily dominates  $\alpha_{xx}$ . For instance,  $Q_{ext,x}^{(1)}$  of the Si<sub>12</sub> and S<sub>10</sub> contribute 92.21% and 96.38% to  $\alpha_{xx}$  value, respectively.  $Q_{ext,x}^{(1)}$  values increase with increasing  $x$ -length, as indicated by the colored regions, while  $\Delta r_{ext,x}^{(1)}$  values are approximately proportional to  $x$ -length, leading to  $\alpha_{xx}$  exponentially dependent on  $x$ -length ( $\alpha_{xx} = Q_{ext,x}^{(1)} \Delta r_{ext,x}^{(1)}$ ). However, the contribution from  $Q_{int,x}^{(1)}$  needs to be considered for longer  $x$ -lengths. For instance,  $Q_{ext,x}^{(1)}$  of the Si<sub>82</sub> and S<sub>70</sub> contribute 62.97% and 75.75% to  $\alpha_{xx}$  value, respectively. In this situation,  $\alpha_{xx}$  can be expressed precisely as:  $\alpha_{xx} = nQ_{int,x}^{(1)p} \Delta r_{int,x}^{(1)p} + Q_{ext,x}^{(1)} \Delta r_{ext,x}^{(1)}$ , where  $Q_{int,x}^{(1)p}$  and  $\Delta r_{int,x}^{(1)p}$  are periodic 1st-response charge and the distance between the positive and negative periodic 1st response-charge centers, and  $n$  refers to periodic numbers.  $Q_{ext,x}^{(1)}$ ,  $Q_{int,x}^{(1)p}$ , and  $\Delta r_{int,x}^{(1)p}$  gradually plateau as  $x$ -length is increased owing to delocalized-electron saturation, while  $\Delta r_{ext,x}^{(1)}$  and  $n$  are precisely proportional to the  $x$ -length, resulting in  $\alpha_{xx}$  linear dependent on  $x$ -length (Figure 3f). Here, 3rd-order response-charge-density curves were not obtained owing to severe numerical errors when performing high-order finite-field calculations. Predictably, the 3rd-order nonlinear optical response characteristics evolving with  $x$ -length are similar to those of linear optical-response characteristics; however,  $Q_{ext,xxx}^{(3)}$  contributing to  $\gamma_{xxx}$  is more significant than  $Q_{ext,x}^{(1)}$  contributing to  $\alpha_{xx}$  at the same  $x$ -length owing to  $Q_{ext,xxx}^{(3)}$  greater sensitivity to electron delocalization.

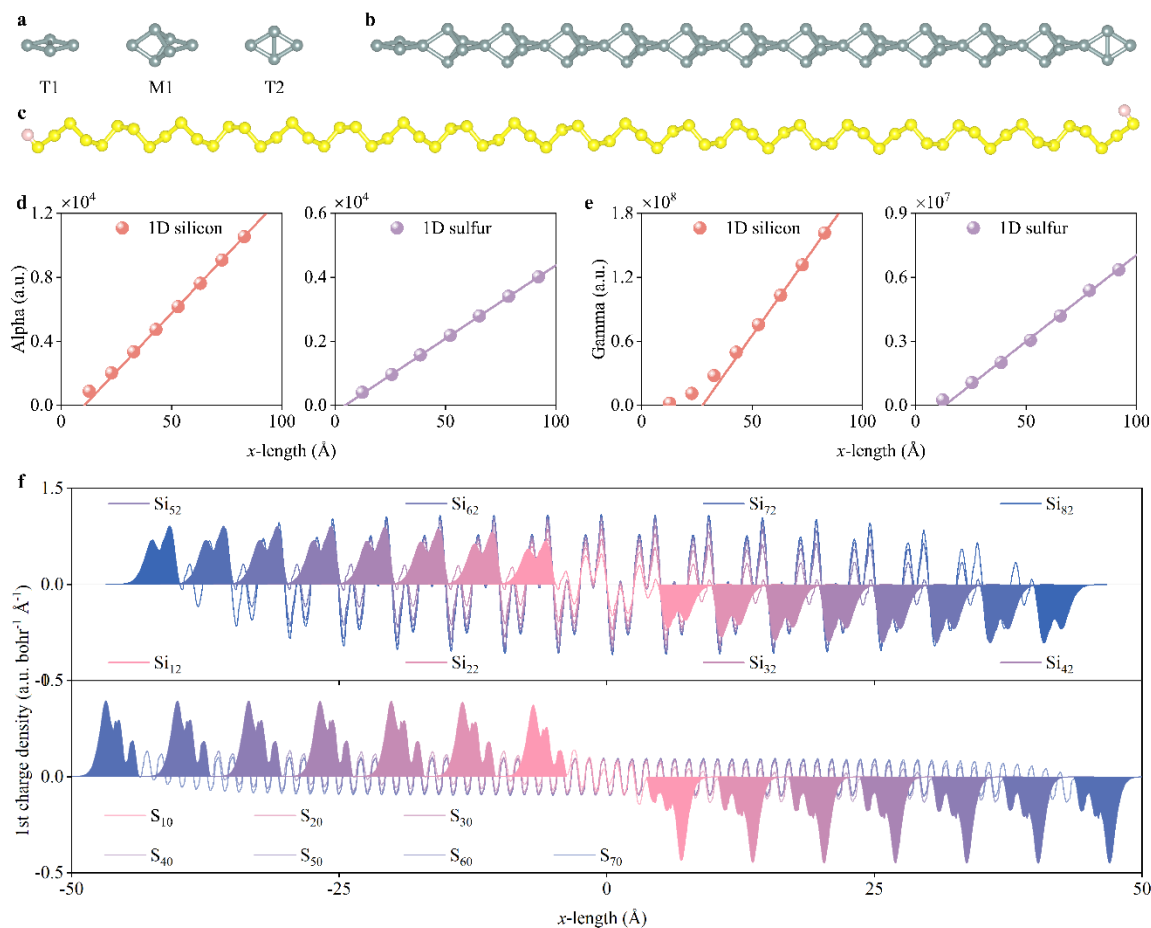


**Figure 3. Linear and nonlinear optical-response characteristics of 1D geometries.** **a**, Fragments T1, T2, and M1 used to assemble 1D silicon geometries. **b**, 1D silicon with  $D_{2d}$  symmetry. **c**, 1D sulfur with helical geometry. Sulfur atoms at endpoint are saturated by hydrogen atoms. **d**, Dependence of  $\alpha_{xx}$  on  $x$ -length for 1D silicon and sulfur. **e**, Dependence of  $\gamma_{xxxx}$  on  $x$ -length for 1D silicon and sulfur. Solid lines are fitted lines that show how  $\alpha_{xx}$  and  $\gamma_{xxxx}$  precisely depend on  $x$ -length following delocalization saturation. **f**, 1st-order response-charge curves for 1D silicon and sulfur at various  $x$ -lengths. Colored regions correspond to 1st-order external response charges.

## CONCLUSIONS

The paradigm explored in this study used an innovative approach to reveal the nonlinear optical behaviors of atomic cluster isomers. Moving away from the traditional multi-level models that are poorly applicable to atomic clusters, the length descriptor (albeit somewhat

simplistically) provides an effective measure of the nonlinear optical performance of an atomic cluster isomer. The introduced response charge was successfully used to demonstrate that lengthening along a dimension enhances electron delocalization in atomic cluster isomers and promotes positive and negative response-charge separation, thereby improving linear and nonlinear optical performance. A simple rule provides effective guidance for experimentalists and theoreticians when designing high-performance nonlinear optical materials, without the need for expensive ab initio calculations or complex machine learning models. Owing to respectable correlations between  $\alpha_{ave}$ ,  $\gamma_{ave}$ , and the length descriptor, this study actually provides a new method for evaluating  $\alpha_{ave}$  and  $\gamma_{ave}$ , which is expected to be useful for predicting the nonlinear optical performance of multi-reference and large systems, as existing theories are unable to satisfactorily evaluate such systems<sup>35</sup>. The length descriptor was shown to provide an effective measure of the linear and nonlinear optical responses of model single-element atomic clusters. Additional parameters are required to accurately determine the optical performance of multi-component atomic clusters because doping modulates the optical response. As is well known, structure substantially and uniquely determines physical properties. Hence, mappings exist between geometric parameters and specific properties, although determining these mappings is challenging. Mapping geometric parameters onto specific properties is a data-driven challenge; however, it is expected to provide a clear physical picture that will greatly promote the development of physics, chemistry, and materials science. This current work represents a preliminary study into the aforementioned concept.

## METHODS

Accurately calculating the  $\alpha$  and  $\gamma$  values of atomic clusters is challenging owing to frequently occurring multi-reference characteristics. Fractional occupation number weighted electron density (FOD) analysis was performed to remove systems with significant multi-reference characteristics<sup>36</sup>. The choice of a reliable exchange-correlation functional for use in DFT calculations when evaluating  $\alpha$  and  $\gamma$  depends on the investigated

systems<sup>37</sup>. A series of calculations were performed to determine an exchange-correlation functional suitable for calculating  $\alpha$  and  $\gamma$ . These measures ensure that a reliable data set was established for analyzing the linear and nonlinear optical-response behaviors of atomic clusters.

Silicon, phosphorus, and sulfur clusters with various initial geometries were generated using the Molclus code<sup>38</sup>. All DFT calculations, excluding FOD calculations, were performed using the Gaussian 16 package<sup>39</sup>, while all MP2 and FOD calculations were performed using the Orca 5.0 package<sup>40</sup>. Numerical differences were analyzed using the Multiwfn program based on files exported by the Gaussian or Orca package<sup>41</sup>. Geometries were rendered using the Visualization for Electronic and STructural Analysis (VESTA) tool<sup>42</sup>.

Atomic-cluster isomers and 1D geometries were optimized to minima on their adiabatic potential energy surfaces using the dispersion corrected PBE0 functional (PBE0-D3(BJ)) in combination with the def2-SVP basis set. The  $\alpha$  and  $\gamma$  components were calculated for atomic cluster isomers at the CAM-B3LYP/aug-cc-pVDZ level, while the  $\alpha$  and  $\gamma$  components of 1D geometries were calculated using the RI-MP2 method paired with the aug-cc-pVDZ basis set. The aug-cc-pVDZ/C auxiliary basis set was chosen for the RI-MP2 calculations, with the integral grid set to DefGrid3. Electron density information required to numerically calculate response charges was generated at the same levels used to calculate  $\alpha$  and  $\gamma$ . SCF convergence criteria were set to  $10^{-8}$  and  $10^{-9}$  a.u. in the Gaussian and Orca packages, respectively. A tighter convergence criterion did not perceptibly improve  $\alpha$  and  $\gamma$ , whereas it hindered convergence. Wavefunction stability was assessed to ensure that all SCF calculations converge to stable wavefunctions. Electric field amplitudes were set to  $10^{-3}$  and  $10^{-4}$  a.u. for response-charge calculations involving atomic-cluster isomers and 1D geometries, respectively. Notably, RI-MP2 introduces non-negligible numerical errors compared to canonical MP2, which are dramatically amplified when performing high-order finite-field calculations<sup>13</sup>. Thus, the 3rd-order response-charge-

density curves of 1D geometries were excluded from the calculations.

## THEORIES

According to Taylor expansion, the  $\alpha$  and  $\gamma$  components can be expressed as follow<sup>29</sup>:

$$\alpha_{il} = - \int \rho_i^{(1)}(\mathbf{r}) l d\mathbf{r}^3 \quad (1)$$

$$\gamma_{ijkl} = - \int \rho_{ijk}^{(3)}(\mathbf{r}) l d\mathbf{r}^3 \quad (2)$$

where  $\rho_i^{(1)}(\mathbf{r}) = [\partial\rho(\mathbf{r})/(\partial F_i)]_{F=0}$ ,  $\rho_{ijk}^{(3)}(\mathbf{r}) = [\partial^3\rho(\mathbf{r})/(\partial F_i\partial F_j\partial F_k)]_{F=0}$ ,  $\rho(\mathbf{r})$  is the electron density,  $F$  is the external electric field,  $i, j, k$  and  $l$  represent one of the directions  $\{x, y, z\}$ ,  $\rho^{(n)}(\mathbf{r})$  is the  $n$ th-order response-charge density, which is conceptually clear despite being referred to as ‘‘hyperpolarizability density’’ in the general literature.  $N$ th-order response charge  $Q^{(n)}$  is introduced in an analogous manner to electron charge  $Q$ . The relationship between  $Q^{(n)}$  and  $\rho^{(n)}(\mathbf{r})$  is clearly expressed as  $dQ^{(n)} = \rho^{(n)}(\mathbf{r})d\mathbf{v}$ .

Furthermore,  $\alpha_{ij}$  and  $\gamma_{ijkl}$  are expressed as follows:

$$\alpha_{il} = Q_i^{(1)}(+)\mathit{r}_l(+)+Q_i^{(1)}(-)\mathit{r}_l(+)\quad (3)$$

$$\gamma_{ijkl} = Q_{ijk}^{(3)}(+)\mathit{r}_l(+)+Q_{ijk}^{(3)}(-)\mathit{r}_l(-)\quad (4)$$

where  $Q^{(n)}(+)$  and  $Q^{(n)}(-)$  refer to the positive and negative response charges, respectively, and  $\mathit{r}_l(+)$  and  $\mathit{r}_l(-)$  represent the coordinate components of the positive and negative response charge distribution centers along the  $l$  direction, respectively.

$Q^{(n)}(+)$  and  $|Q^{(n)}(-)|$  are precisely equal for electrically neutral systems; consequently,  $\alpha_{ij}$  and  $\gamma_{ijkl}$  are further expressed as:

$$\alpha_{il} = Q_i^{(1)}\Delta\mathit{r}_l^{(1)}\quad (5)$$

$$\gamma_{ijkl} = Q_{ijk}^{(3)}\Delta\mathit{r}_l^{(3)}\quad (6)$$

where  $Q^{(n)}$  is the  $n$ th-order response charge and  $\Delta\mathit{r}_l^{(n)}$  is the distance between the  $n$ th-order positive and negative response charge distribution centres along the  $l$  direction.

## ACKNOWLEDGEMENTS

The author especially thanks his family, without whose support this work would not have been completed.

## REFERENCES

- [1] Tsukamoto, T.; Kambe, T.; Imaoka, T.; Yamamoto, K., Modern cluster design based on experiment and theory. *Nature Reviews Chemistry* **2021**, *5* (5), 338–347.
- [2] Zhao, J.; Du, Q.; Zhou, S.; Kumar, V., Endohedrally doped cage clusters. *Chemical Reviews* **2020**, *120* (17), 9021–9163.
- [3] Jena, P.; Sun, Q., Super atomic clusters: Design rules and potential for building blocks of materials. *Chemical Reviews* **2018**, *118* (11), 5755–5870.
- [4] Zheng, J.; Zhang, C.; Dickson, R. M., Highly fluorescent, water-soluble, size-tunable gold quantum dots. *Physical Review Letters* **2004**, *93* (7), 077402.
- [5] Ramakrishna, G.; Varnavski, O.; Kim, J.; Lee, D.; Goodson, T., Quantum-sized gold clusters as efficient two-photon absorbers. *Journal of the American Chemical Society* **2008**, *130* (15), 5032–5033.
- [6] Pan, P.; Liu, L.; Zhang, L.; Wei, X.; Tian, Y.; Kang, X.; Zhang, Q.; Zhu, M., Control the single-, two-, and three-photon excited fluorescence of atomically precise metal nanoclusters. *Angewandte Chemie International Edition* **2022**, *61* (50), e202213016.
- [7] Gao, M.-Y.; Wang, Z.; Li, Q.-H.; Li, D.; Sun, Y.; Andaloussi, Y. H.; Ma, C.; Deng, C.; Zhang, J.; Zhang, L., Black titanium-oxo clusters with ultralow band gaps and enhanced nonlinear optical performance. *Journal of the American Chemical Society* **2022**, *144* (18), 8153–8161.
- [8] Hou, H.; Wei, Y.; Song, Y.; Mi, L.; Tang, M.; Li, L.; Fan, Y., Metal ions play different roles in the third-order nonlinear optical properties of  $d^{10}$  metal–organic clusters. *Angewandte Chemie International Edition* **2005**, *117* (37), 6221–6228.
- [9] Chen, W.; Li, Z.-R.; Wu, D.; Li, Y.; Sun, C.-C.; Gu, F. L.; Aoki, Y., Nonlinear optical properties of alkalides  $\text{Li}^+$  (calix [4] pyrrole)  $\text{M}^-$  ( $\text{M} = \text{Li}, \text{Na}, \text{and K}$ ): Alkali anion

atomic number dependence. *Journal of the American Chemical Society* **2006**, *128* (4), 1072–1073.

- [10] Wang, Z.-K.; Du, M.-H.; Braunstein, P.; Lang, J.-P., A cut-to-link strategy for cubane-based heterometallic sulfide clusters with giant third-order nonlinear optical response. *Journal of the American Chemical Society* **2023**, *145* (18), 9982–9987.
- [11] Luo, M.-B.; Lai, H.-D.; Huang, S.-L.; Zhang, J.; Lin, Q., Pseudotetrahedral organotin-capped chalcogenidometalate supermolecules with optical limiting performance. *Journal of the American Chemical Society* **2024**, *146* (11), 7690–7697.
- [12] Kaka, K. S.; Beaujean, P.; Castet, F.; Champagne, B., A quantum chemical investigation of the second hyperpolarizability of *p*-nitroaniline. *The Journal of Chemical Physics* **2023**, *159* (11), 114104.
- [13] Naim, C.; Besalú-Sala, P.; Zalesny, R.; Luis, J. M.; Castet, F.; Matito, E., Are accelerated and enhanced wave function methods accurate to compute static linear and nonlinear optical properties? *Journal of Chemical Theory and Computation* **2023**, *19* (6), 1753–1764.
- [14] Mutailipu, M.; Han, J.; Li, Z.; Li, F.; Li, J.; Zhang, F.; Long, X.; Yang, Z.; Pan, S., Achieving the full-wavelength phase-matching for efficient nonlinear optical frequency conversion in  $C(NH_2)_3BF_4$ . *Nature Photonics* **2023**, *17* (8), 694–701.
- [15] Abudurusuli, A.; Huang, J.; Wang, P.; Yang, Z.; Pan, S.; Li, J.,  $Li_4MgGe_2S_7$ : The first alkali and alkaline-earth diamond-like infrared nonlinear optical material with exceptional large band gap. *Angewandte Chemie International Edition* **2021**, *60* (45), 24131–24136.
- [16] Kuzyk, M. G.; Perez-Moreno, J.; Shafei, S., Sum rules and scaling in nonlinear optics. *Physics Reports* **2013**, *529* (4), 297–398.
- [17] Lytel, R.; Mossman, S.; Crowell, E.; Kuzyk, M. G., Exact fundamental limits of the first and second hyperpolarizabilities. *Physical Review Letters* **2017**, *119* (7), 073902.
- [18] Kang, H.; Facchetti, A.; Jiang, H.; Cariati, E.; Righetto, S.; Ugo, R.; Zuccaccia, C.;

Macchioni, A.; Stern, C. L.; Liu, Z.; Ho, S.-T.; Brown, E. C.; Ratner, M. A.; Marks, T. J., Ultralarge hyperpolarizability twisted  $\pi$ -electron system electro-optic chromophores: Synthesis, solid-state and solution-phase structural characteristics, electronic structures, linear and nonlinear optical properties, and computational studies. *Journal of the American Chemical Society* **2007**, *129* (11), 3267–3286.

[19] Hales, J. M.; Matichak, J.; Barlow, S.; Ohira, S.; Yesudas, K.; Brédas, J.-L.; Perry, J. W.; Marder, S. R., Design of polymethine dyes with large third-order optical nonlinearities and loss figures of merit. *Science* **2010**, *327* (5972), 1485–1488.

[20] Jiang, Y.; Gindre, D.; Allain, M.; Liu, P.; Cabanetos, C.; Roncali, J., A mechanofluorochromic push-pull small molecule with aggregation-controlled linear and nonlinear optical properties. *Advanced Materials* **2015**, *27* (29), 4285–4289.

[21] Zhong, Q., Size-dependent linear and nonlinear optical responses of silicon clusters. *Physical Chemistry Chemical Physics* **2024**, *26* (7), 6022–6028.

[22] Giesecking, R. L. M., Third-order nonlinear optical properties of Ag nanoclusters: Connecting molecule-like and nanoparticle-like behavior. *Chemistry of Materials* **2019**, *31* (17), 6850–6859.

[23] Zhong, Q., Lone-pair, electron-dominated, nonlinear optical responses in sulfur clusters and electric tunability properties. *Physical Chemistry Chemical Physics* **2023**, *25* (42), 29120–29126.

[24] Wang, Z.; Zhao, G.; Yan, W.; Wu, K.; Wang, F.; Li, Q.; Zhang, J., Tin metal cluster compounds as new third-order nonlinear optical materials by computational study. *The Journal of Physical Chemistry Letters* **2021**, *12* (31), 7537–7544.

[25] Tkatchenko, A.; Scheffler, M., Accurate molecular van der Waals interactions from ground-state electron density and free-atom reference data. *Physical Review Letters* **2009**, *102* (7), 073005.

[26] Blair, S. A.; Thakkar, A. J., Relating polarizability to volume, ionization energy, electronegativity, hardness, moments of momentum, and other molecular properties.

*The Journal of Chemical Physics* **2014**, *141* (7), 074306.

- [27] Puccetti, G.; Blanchard-Desce, M.; Ledoux, I.; Lehn, J. M.; Zyss, J., Chain-length dependence of the third-order polarizability of disubstituted polyenes: effects of end groups and conjugation length. *The Journal of Physical Chemistry* **1993**, *97* (37), 9385–9391.
- [28] Eisler, S.; Slepko, A. D.; Elliott, E.; Luu, T.; McDonald, R.; Hegmann, F. A.; Tykwinski, R. R., Polyynes as a model for carbyne: synthesis, physical properties, and nonlinear optical response. *Journal of the American Chemical Society* **2005**, *127* (8), 2666–2676.
- [29] Nakano, M.; Shigemoto, I.; Yamada, S.; Yamaguchi, K., Size-consistent approach and density analysis of hyperpolarizability: Second hyperpolarizabilities of polymeric systems with and without defects. *The Journal of Chemical Physics* **1995**, *103* (10), 4175–4191.
- [30] Zhong, Q., Lone pair electrons with weak nuclear binding inducing sensitive nonlinear optical responses in phosphorus clusters. *The Journal of Physical Chemistry Letters* **2023**, *14* (28), 6361–6367.
- [31] Cohen, A. J.; Mori-Sánchez, P.; Yang, W., Insights into current limitations of density functional theory. *Science* **2008**, *321* (5890), 792–794.
- [32] Ho, K.-M.; Shvartsburg, A. A.; Pan, B.; Lu, Z.-Y.; Wang, C.-Z.; Wacker, J. G.; Fye, J. L.; Jarrold, M. F., Structures of medium-sized silicon clusters. *Nature* **1998**, *392* (6676), 582–585.
- [33] Steudel, R.; Eckert, B., Solid sulfur allotropes. *Elemental sulfur and sulfur-rich compounds I* **2003**, 1–80.
- [34] Thienpont, H.; Rikken, G. L. J. A.; Meijer, E. W.; ten Hoeve, W.; Wynberg, H., Saturation of the hyperpolarizability of oligothiophenes. *Physical Review Letters* **1990**, *65* (17), 2141–2144.
- [35] Löffelsender, S.; Beaujean, P.; de Wergifosse, M., Simplified quantum chemistry

- methods to evaluate non-linear optical properties of large systems. *Wiley Interdisciplinary Reviews: Computational Molecular Science* **2024**, *14* (1), e1695.
- [36] Grimme, S.; Hansen, A., A practicable real-space measure and visualization of static electron-correlation effects. *Angewandte Chemie International Edition* **2015**, *54* (42), 12308–12313.
- [37] Champagne, B.; Perpete, E. A.; van Gisbergen, S. J. A.; Baerends, E.-J.; Snijders, J. G.; Soubra-Ghaoui, C.; Robins, K. A.; Kirtman, B., Assessment of conventional density functional schemes for computing the polarizabilities and hyperpolarizabilities of conjugated oligomers: An ab initio investigation of polyacetylene chains. *The Journal of Chemical Physics* **1998**, *109* (23), 10489–10498.
- [38] Lu, T., Molclus program, Version 1.12, <http://www.keinsci.com/research/molclus.html> (accessed June 1, 2024).
- [39] Frisch, M. J.; Trucks, G. W.; Schlegel, H. B.; Scuseria, G. E.; Robb, M. A.; Cheeseman, J. R.; Scalmani, G.; Barone, V.; Petersson, G. A.; Nakatsuji, H.; Li, X.; Caricato, M.; Marenich, A. V.; Bloino, J.; Janesko, B. G.; Gomperts, R.; Mennucci, B.; Hratchian, H. P.; Ortiz, J. V.; Izmaylov, A. F.; Sonnenberg, J. L.; Williams, Ding, F.; Lipparini, F.; Egidi, F.; Goings, J.; Peng, B.; Petrone, A.; Henderson, T.; Ranasinghe, D.; Zakrzewski, V. G.; Gao, J.; Rega, N.; Zheng, G.; Liang, W.; Hada, M.; Ehara, M.; Toyota, K.; Fukuda, R.; Hasegawa, J.; Ishida, M.; Nakajima, T.; Honda, Y.; Kitao, O.; Nakai, H.; Vreven, T.; Throssell, K.; Montgomery Jr., J. A.; Peralta, J. E.; Ogliaro, F.; Bearpark, M. J.; Heyd, J. J.; Brothers, E. N.; Kudin, K. N.; Staroverov, V. N.; Keith, T. A.; Kobayashi, R.; Normand, J.; Raghavachari, K.; Rendell, A. P.; Burant, J. C.; Iyengar, S. S.; Tomasi, J.; Cossi, M.; Millam, J. M.; Klene, M.; Adamo, C.; Cammi, R.; Ochterski, J. W.; Martin, R. L.; Morokuma, K.; Farkas, O.; Foresman, J. B.; Fox, D. J. *Gaussian 16*, Wallingford, CT, **2016**.
- [40] Neese, F., Software update: The ORCA program system—Version 5.0. *Wiley Interdisciplinary Reviews: Computational Molecular Science* **2022**, *12* (5), e1606.

- [41]Lu, T.; Chen, F., Multiwfn: A multifunctional wavefunction analyzer. *Journal of Computational Chemistry* **2012**, *33* (5), 580–592.
- [42]Momma, K.; Izumi, F., VESTA 3 for three-dimensional visualization of crystal, volumetric and morphology data. *Journal of Applied Crystallography* **2011**, *44* (6), 1272–1276.